Decaying two-dimensional turbulence in square containers with no-slip or stress-free boundaries

Decaying two-dimensional turbulence in square containers with no-slip or stress-free boundaries

H. J. H. Clercx, S. R. Maassen, and G. J. F. van Heijst
Department of Physics, Eindhoven University of Technology, P.O. Box 513, 5600 MB Eindhoven, The Netherlands

(Received 29 July 1997; accepted 18 November 1998)

We report results of direct numerical simulations of decaying two-dimensional (2D) turbulence inside a square container with rigid boundaries. It is shown that the type of boundary condition (no-slip or stress-free) determines the flow evolution essentially. During the initial ($0 \leqslant t \leqslant 0.2\sqrt{\mathrm{Re}}$) and intermediate ($0.2\sqrt{\mathrm{Re}} \leqslant t \leqslant 3\sqrt{\mathrm{Re}}$) stages of decaying 2D turbulence ($t \cong 1$ is comparable with an eddy turnover time, Re is the Reynolds number of the flow), the decay scenario for simulations with no-slip boundary conditions can be understood from turbulent spectral transfer and selective decay. A third mechanism can be recognized for $t \geqslant 3\sqrt{\mathrm{Re}}$: A decay stage where diffusion dominates over nonlinear advection, i.e., spectral transfer is then absent in favor of self-similar decay. The present results show that at presently accessible Reynolds numbers and computation times, laboratory experiments cannot be accurately compared with quasi-stationary states from ideal maximum-entropy theories or with computed solutions of flows in containers with stress-free boundaries. The decay which results in rectangular containers with no-slip boundaries does not yet yield anything that is meaningfully comparable with these formulations. The evolution of the number of vortices V, the average vortex radius a, the ratio of enstrophy Ω over energy E, and the extremum of vorticity (normalized by $\sqrt{E}$) have been computed based on ensemble averaging of the no-slip runs. An algebraic regime has been observed with $V(t) \sim t^{-0.90}$, $a(t) \sim t^{0.31}$, $\Omega(t)/E(t) \sim t^{-0.63}$, and $\omega_{\mathrm{ext}}(t)/\sqrt{E(t)} \sim t^{-0.30}$. Finally, quantities such as a measure of the viscous stresses near the boundaries have been computed in order to analyze the decay of 2D turbulence in containers with rigid boundaries. © *1999 American Institute of Physics.* [S1070-6631(99)01403-8]

I. INTRODUCTION

High-resolution numerical simulations of decaying two-dimensional (2D) turbulence have revealed many interesting features concerning flow dynamics, inertial range energy spectra, mixing properties of the flow, passive tracer dynamics, etc. Two specific aspects of the flow dynamics of decaying 2D turbulence are relevant in the context of the numerical simulations reported in this paper. The first one concerns the formation of small-scale structures in the form of vorticity-gradient sheets at early times of the flow evolution, a property of the flow dynamics nicely illustrated in high-resolution numerical simulations of decaying 2D turbulence on a double-periodic domain by, e.g., Brachet *et al.*[1,2] During the later stage of the flow evolution another characteristic aspect of decaying 2D turbulence is observed: The emergence of coherent vortices. This process has been shown in direct numerical simulations of decaying 2D turbulence on a double-periodic domain by, for example, Matthaeus and Montgomery,[3] who reported for the first time on large-scale convection cells in a Navier–Stokes simulation with periodic boundary conditions, by McWilliams,[4] and by Santangelo, Benzi, and Legras.[5] During a long-time integration of the Navier–Stokes equations, Matthaeus *et al.*[6] observed the appearance of a quasi-steady final state consisting of two vortices with opposite circulation.

Numerical studies of decaying 2D turbulence are generally based on simulations of the Navier–Stokes equations for incompressible flows on a square domain with periodic boundary conditions. We report here on results of numerical simulations of decaying 2D turbulent flows on a square domain with impermeable boundaries, for Reynolds numbers up to 2000 with either *no-slip* or *stress-free* boundary conditions. The definition of the Reynolds number in the present simulations is based on the root-mean-square (rms) velocity of the initial flow field and the half-width of the domain. Simulations of the full 2D Navier–Stokes equations, i.e., without artificial dissipation replacing diffusion, are carried out with a 2D Chebyshev pseudospectral algorithm with a maximum of 289 Chebyshev modes in both directions.

The present numerical study of decaying 2D turbulence in a container with rigid boundaries is primarily motivated by laboratory observations. Examples are the experimental studies of decaying 2D turbulence in stratified fluids, observations of strong vortex–wall interactions in bounded quasi-2D flows, and the emergence of large-scale counter-rotating vortices in rectangular containers with the vortex radii comparable with the width of the container. Experiments on 2D turbulence have been carried out in rectangular, square, or circular containers filled with fluid. The containers were either rotating (see Ref. 7 and references therein) or filled with a linearly stratified or a two-layer fluid.[8–10] The initial random flow field in stratified fluids was obtained by stirring with a rake,[8] or by using sources and sinks, as was

done in the experiments by Boubnov, Dalziel, and Linden.[10] Alternative techniques for investigating 2D flow dynamics are based on electromagnetic forcing mechanisms. Examples are the experiments by Nguyen Duc and Sommeria[11] with a shallow layer of mercury subjected to magnetic forcing and the electromagnetically forced electrolyte solutions used in experiments by Tabeling *et al.*[12] and Marteau, Cardoso, and Tabeling.[13] In all these cases, the flows were bounded by walls, at which no-slip conditions apply. Several theoretical approaches for investigating 2D flows take into account the presence of impermeable boundaries, although neither of them of no-slip type. Examples are the study by Pointin and Lundgren[14] on the statistical mechanics of 2D vortices in a bounded container and the classification study of self-organized structures in 2D turbulence in perfect fluids (Euler flows) by Chavanis and Sommeria.[15] The latter approach is based on an application of a maximum entropy theory.[16,17] A description in terms of the maximum entropy principle has also been used for the coherent structures appearing in computed solutions of 2D decaying Navier–Stokes flow with periodic boundary conditions.[18–20] Additionally, numerical simulations of decaying 2D turbulence in containers with rigid stress-free walls have been reported.[21,22] These theoretical and numerical studies concerned flows in containers with free-slip or stress-free boundaries, leaving the question unanswered as to what extent realistic, no-slip boundary conditions play a role in the flow evolution. A comparison between the decay process of 2D turbulence in the presence of no-slip and stress-free boundary conditions seems worthwhile in order to show the entirely different flow evolution in both cases, owing to the crucial role of the boundary layers in the flow dynamics in containers with no-slip boundaries.

Recently, Li and Montgomery[23] and Li, Montgomery, and Jones[24,25] have reported results of computations of decaying 2D turbulence inside a circular rigid boundary. Simulations with no-slip boundaries and an initial velocity field containing a large amount of net angular momentum L revealed a very slow decay of L, and the presence of angular momentum in the initial flow field seems to play a crucial role in the flow evolution.[24] For this case, the quasi-stationary intermediate state consists of a monopolar vortex in the center of the circular container. In contrast, runs with $L(t=0)=0$ (and which remains approximately zero during the decay of 2D turbulence) showed the eventual formation of an intermittent dipolar structure. The vorticity produced in the boundary layer between the dipole and the no-slip boundary is predominantly accumulated in the wake of the dipole.

The organization of this paper is as follows: The governing equations in dimensionless form, the time discretization scheme, and the spatial approximation by a Chebyshev pseudospectral method are recalled in Sec. II. Additionally, numerical convergence is briefly discussed. Results of numerical simulations of decaying 2D turbulence with no-slip boundary conditions are presented in Sec. III, and in Sec. IV the decay scenarios for numerical simulations with no-slip and with stress-free boundary conditions are compared. In Sec. V the results and conclusions are summarized.

II. NUMERICAL ALGORITHM AND INITIALIZATION PROCEDURE

Numerical simulations are performed with a 2D Chebyshev pseudospectral method which is here only briefly reviewed. Technical details of the numerical code are described elsewhere.[26] The flow domain D with boundary ∂D is a two-dimensional square cavity—in dimensionless form the square $[-1,1]\times[-1,1]$, Cartesian coordinates in a frame of reference are denoted by x and y, and the velocity field is denoted by $\mathbf{u}=(u,v)$. The equation governing the nondimensional (scalar) vorticity $\omega=(\partial v/\partial x)-(\partial u/\partial y)$ is obtained by taking the curl of the momentum equation. The following set of equations has to be solved numerically:

$$\frac{\partial \omega}{\partial t}+(\mathbf{u}\cdot\nabla)\omega=\frac{1}{\mathrm{Re}}\nabla^2\omega \quad \text{in } D,$$
$$\nabla^2\mathbf{u}=\mathbf{k}\times\nabla\omega \quad \text{in } D, \tag{1}$$

with the boundary condition $\mathbf{u}=\mathbf{u}_b$ ($\mathbf{u}_b=0$ for no-slip boundaries) and enforcing $\mathbf{k}\cdot\nabla\times\mathbf{u}=\omega$ on ∂D by an influence matrix method.[26] An initial condition, $\omega|_{t=0}=\mathbf{k}\cdot\nabla\times\mathbf{u}_i$, where $\mathbf{u}_i$ is the initial velocity field, is also supplemented. The Reynolds number is defined as $\mathrm{Re}=UW/\nu$, with U a characteristic velocity (based on the rms velocity of the initial flow field), W the half-width of the box and ν the kinematic viscosity of the fluid. The time is made dimensionless with W/U, and $t\cong 1$ is comparable with an eddy turnover time. Time discretization of the vorticity equation [Eq. (1)] is semi-implicit: It uses the explicit Adams–Bashforth scheme for the advection term and the implicit Crank–Nicolson procedure for the diffusive term. Both components of the velocity and the vorticity are expanded in a double truncated series of Chebyshev polynomials, e.g., for the velocity field:

$$\mathbf{u}(x,y,t)=\sum_{n=0}^{N}\sum_{m=0}^{N}\hat{\mathbf{u}}_{nm}(t)T_n(x)T_m(y), \tag{2}$$

where the Chebyshev polynomials $T_n(x)=\cos(n\theta)$ with $\theta=\cos^{-1}(x)$. Transformations from physical space to the spectral space of expansion coefficients, and vice versa, can be performed efficiently by employing fast Fourier transform (FFT) methods. All numerical calculations, except the evaluation of the nonlinear terms, are performed in spectral space, i.e., the coefficients $\hat{\mathbf{u}}_{nm}(t)$ and $\hat{\omega}_{nm}(t)$ are marched in time. FFT methods are used to evaluate the nonlinear terms following the procedure designed by Orszag,[27] where the padding technique has been used for de-aliasing.

The initial condition for the velocity field, denoted by $\mathbf{u}_i$, is obtained by a zero-mean Gaussian random realisation of the first 65×65 Chebyshev spectral coefficients of both u_i and v_i, and subsequently applying a smoothing procedure in order to enforce $\mathbf{u}_i=0$ at the boundary of the domain. The variance σ_{nm} of the velocity spectrum of $\mathbf{u}_i$ is chosen as

$$\sigma_{nm}^2=\frac{n}{[1+(\frac{1}{8}n)^4]}\,\frac{m}{[1+(\frac{1}{8}m)^4]}, \quad \text{with } 0\leqslant n,m\leqslant 64, \tag{3}$$

and $\sigma_{nm} \equiv 0$ for $n,m \geqslant 65$, and the resulting flow field is denoted by $\mathbf{U}(x,y)$. The smoothing function is $f(x)=[1-\exp(-\beta(1-x^2)^2)]$, with $\beta=100$. The initial velocity field is thus: $\mathbf{u}_i(x,y)=f(x)f(y)\mathbf{U}(x,y)$, where the flow field is normalized in order to enforce the L^2-norm of the velocity per unit surface of the initial flow field to be equal to unity. The kinetic energy and the enstrophy of the flow are defined as

$$E=\frac{1}{2}\int_{-1}^{1}\int_{-1}^{1}[u^2(x,y)+v^2(x,y)]dxdy, \tag{4}$$

$$\Omega=\frac{1}{2}\int_{-1}^{1}\int_{-1}^{1}\omega^2(x,y)dxdy. \tag{5}$$

It should be emphasized that for all numerical runs the kinetic energy of the flow field drops from $E(t=0)=2$ [see Eq. (4)] to $E(t=0^+)\cong 1$ during the first time integration step, because the initial velocity field, with $\nabla\cdot\mathbf{u}_i\neq 0$, is then projected onto the subspace of divergence-free velocity fields. Values for the energy and enstrophy during the simulations are normalized with their values obtained after the first time integration step. A more proper treatment for obtaining a divergence-free initial velocity field is discussed in a review paper by Gresho,[28] but for the present simulations the procedure described above is sufficient; the details of the initial flow field are not important.

The angular momentum of the flow, defined with respect to the center of the container, is

$$L=\mathbf{k}\cdot\int_{-1}^{1}\int_{-1}^{1}\mathbf{r}\times\mathbf{u}(x,y)dxdy$$

$$=2\int_{-1}^{1}\int_{-1}^{1}\psi(x,y)dxdy, \tag{6}$$

with the stream function ψ defined in the usual way, $u=\partial\psi/\partial y$ and $v=-\partial\psi/\partial x$. The right-hand side (rhs) of Eq. (6) is obtained by using the condition that ψ is constant at the boundary of the domain (actually, we set $\psi=0$ on ∂D). Due to the initialization procedure of the flow field, the total angular momentum at $t=0$ is not exactly zero, but still small. However, the mean value of the total angular momentum over a large number of realizations is zero.

Simulations have been carried out for three values of the Reynolds number: Re=1000, 1500, and 2000. As a first step, the minimum number of Chebyshev modes required in order to get a well-resolved simulation of the flow dynamics, has been investigated. The qualification ''well-resolved'' means that the smallest scales are resolved and that the decay process becomes effectively independent of a further increase of the number of degrees of freedom used in the numerical simulations. In all numerical experiments it appeared that the convergence criterion results in a minimum number of Chebyshev modes which is roughly proportional with $\sqrt{\mathrm{Re}}$ in each direction (see Table I where also other relevant information for the runs with no-slip and stress-free boundaries is summarized). This observation is consistent with analyses reported in the literature for homogeneous, isotropic 2D turbulence, where it has been shown that the total number of degrees of freedom ($N\times N$) of 2D turbulence is of the order of the Reynolds number. A fit through the data from Table I in a log–log plot of Reynolds number versus number of Chebyshev modes gives roughly: $N\cong 6\sqrt{\mathrm{Re}}$. These experimentally obtained minimum numbers of Chebyshev modes are consistent with the requirement that the dimensionless dissipation wave number $\mathbf{k}_d=2\pi\lambda_d^{-1}=W(\epsilon/\nu^3)^{1/6}$, with ϵ the instantaneous enstrophy decay rate per unit area, is sufficiently lower than N. This relation can be written as $\lambda_d \cong 8\,\mathrm{Re}^{-1/2}\overline{\epsilon}^{-1/6}>2/N$, with $\overline{\epsilon}$ the dimensionless enstrophy decay rate (as obtained from the computations). With $N\cong 6\sqrt{\mathrm{Re}}$, the following relation is found for the dimensionless enstrophy decay rate: $\overline{\epsilon}<2\times 10^8$. This condition is always satisfied for the runs discussed here (see Table I where estimated values for $\overline{\epsilon}$ are listed).

TABLE I. Characteristics of the runs presented in this paper; these parameters were the same for the runs with no-slip and with stress-free boundary conditions.

Re	N	Time step	Latest time	$\overline{\epsilon}_{\max}$
500	128	2.5×10^{-4}	400	2×10^6
1000	180	2.5×10^{-4}	400	8×10^6
1500	216	1.5×10^{-4}	400	2×10^7
2000	288	1.25×10^{-4}	400	5×10^7

III. COMPUTATIONAL RESULTS; NO-SLIP BOUNDARY CONDITIONS

A. General features

The flow evolution of decaying 2D turbulence on a square domain with no-slip boundary conditions can be characterized, at least up to Re=2000, by three stages (the relevant time scales associated with these stages are discussed in Sec. III B). The *initial stage* consists of a rapid self-organization process due to merging of like-sign vortices and the formation of mainly medium-sized dipoles. This process is nicely illustrated in Figs. 1(a)–1(d) where vorticity contour plots from a simulation of freely decaying 2D turbulence with Re=2000 are presented. Average scales present in the random initial vorticity field have characteristic length scales λ that are roughly two orders of magnitude smaller than the container size, i.e., $\lambda(t=0)\cong 0.01W$. The average size of the vortices increases rapidly to $\lambda(t=1)\cong 0.2W$ and to $\lambda(t=5)\cong 0.4W$ [see Figs. 1(a)–1(c)]. The self-organization process is accompanied by the formation and steepening of vorticity gradients by strain in the interior due to vortex interactions, and the formation of boundary layers due to shear near no-slip walls. The intense vorticity filaments produced in the boundary layer are either injected into the flow interior, where they are elongated in strain-dominated parts of the flow field, resulting in thin vorticity gradient sheets, or they roll up into a vorticity blob. In the latter case they usually pair with the neighboring (primary) vortex, thus forming a dipolar structure. This process becomes increasingly important as from $t\cong 1$ [see Figs. 1(a) and 1(b)] when sufficiently strong dipoles have been formed. Boundary layer detachment and subsequent advection into

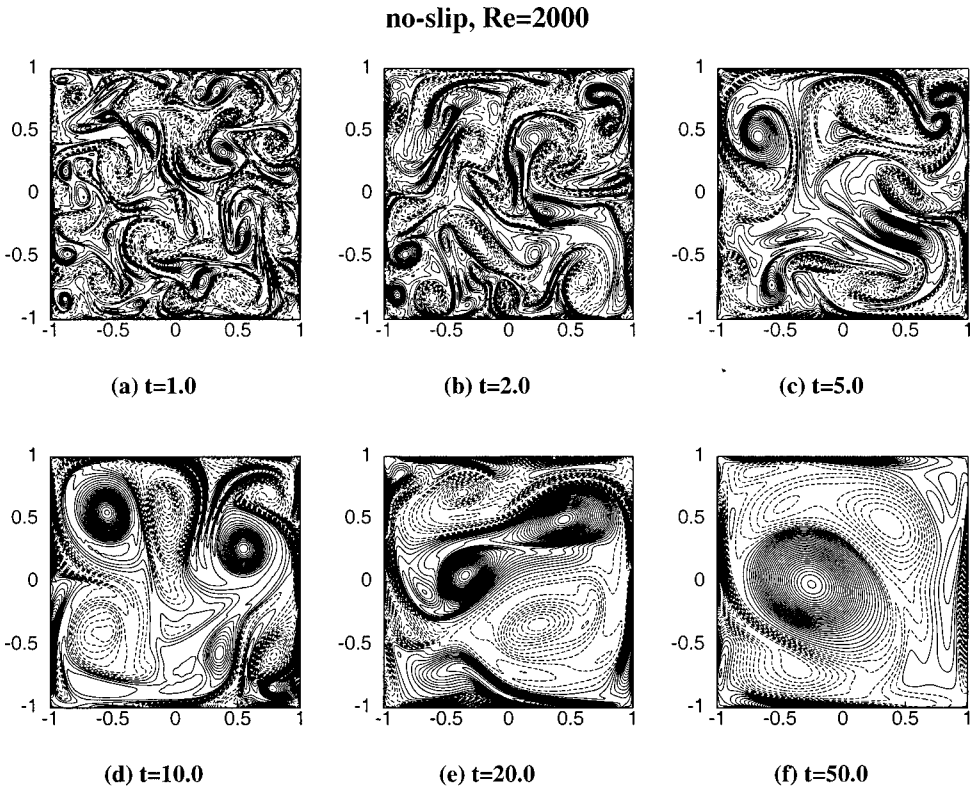

FIG. 1. Vorticity contour plots of a simulation with no-slip boundary conditions, Re=2000. Dashed contours represent negative vorticity, and drawn contours represent positive vorticity. The contour level increment is: (a) 3, (b) 1.5, (c) 0.75, (d) 0.4, (e) 0.2, and (f) 0.1.

the interior of the flow is clearly observed in Figs. 1(c)–1(e) ($t \cong 5$, 10, and 20, respectively). The higher the Reynolds number, the longer this process of boundary layer detachment and dipole formation continues. The *second stage* is characterized by the presence of strong vortex–wall interactions and the formation of coherent structures with sizes comparable with the container dimension [see Figs. 1(e) and 1(f)]. During this stage, the absolute value of the angular momentum of the flow often increases rapidly, and decays afterwards only very slowly. This sudden increase of the angular momentum reflects the *spontaneous spin-up* of the flow.[29] To illustrate this phenomenon, the angular momentum for two simulations with Re=2000, which show spontaneous spin-up, is plotted in Fig. 2 (the upper curve corresponds to the run shown in Fig. 1). It is worthwhile to note that the angular momentum of the same amount of fluid, with total kinetic energy $E=1$, in solid body rotation is $|L_{sb}| \cong 2.3$. Since the angular momentum of unbounded viscous flows is conserved when the total circulation (as in bounded domains with no-slip walls) is zero, the spontaneous spin-up of the flow is a process which is entirely due to the finiteness of the flow. A practical implication of the spin-up phenomenon is that a torque needs to be exerted on the container in order to prevent spontaneous rotation of the container, since the total angular momentum of the torque-free fluid-container system is conserved. Several runs have been carried out with Re=1000, 1500, and 2000 (see Table II) and approximately 75% of these runs shows spontaneous spin-up. The flow during the intermediate stage is then always characterized by the presence of a strong monopolar or a rotating tripolar structure. A small minority of the runs shows no spin-up at all, and during the intermediate stage of these runs usually a dipolar or quadrupolar structure is found. The *third stage* is characterized by a relaxation process to a monopolar structure that is more or less situated in the center of the container, subsequently followed by viscous relaxation.

Two important processes for the self-organization of the flow are the spectral transfer due to nonlinear interactions and the selective decay hypothesis, which states that higher spectral components, which are excited by turbulent spectral transfer, dissipate more rapidly than the lower spectral

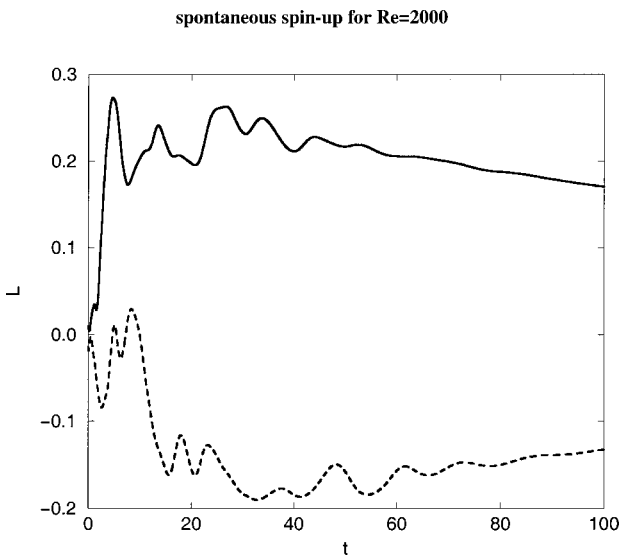

FIG. 2. The angular momentum L plotted vs dimensionless time t for Re =2000 for two typical runs that show spontaneous spin-up.

TABLE II. Several characteristics obtained from ensemble simulations of decaying 2D turbulence in square containers with no-slip boundaries. The characteristic spin-up times and amplitudes are based on averages of the runs showing spontaneous spin-up.

	Re=1000	Re=1500	Re=2000
total number of runs:	12	12	13
spontaneous spin-up:	7	8	8
weak spin-up:	1	2	3
no spin-up:	4	2	2
spin-up time:	12	20	17
spin-up amplitude:	0.14	0.20	0.22

components.[3] These two processes are responsible for a spectral accumulation at the lowest frequencies. Recently, a third important process during nonlinear self-organization has been recognized by Kondoh *et al.*[21] for incompressible viscous flow with stress-free boundary conditions ($\omega=0$ on ∂D). This process consists of the interchange of dominance between the two physical processes which determine the flow evolution. The early and intermediate decay stages are predominantly determined by the action of the nondissipative nonlinear term, but in the later stage of decay the dissipative term becomes dominant. As a result, the lowest eigenmode solution of the vorticity diffusion equation on a bounded square domain with stress-free boundary conditions should finally emerge, because it is the mode with the smallest damping factor. The lowest eigenmode solution decays then self-similarly. Such eigenmode solutions were recently calculated for viscous flow on a square domain with no-slip boundaries by Van de Konijnenberg, Flór, and van Heijst,[9] and they are used in the present investigation to analyse the long-time decay properties of freely evolving 2D turbulence.

An important tool to quantify the self-organization process is the spectrum, which provides insight into the distribution of kinetic energy of the flow over the different modes. Standard techniques exist to determine the spectrum for forced or decaying 2D turbulence with periodic boundary conditions. Unfortunately, such techniques cannot be applied straightforwardly when rigid boundaries are present. An approach might be the calculation of the spectrum of eigenmodes of viscous flow on a square domain with no-slip boundaries. However, this method is rather elaborate (see Van de Konijnenberg *et al.*[9]). An alternative is to measure the so-called one-dimensional spectrum of Chebyshev modes. This approach does not provide all information on spectral transfer, because it is merely an average, but it still gives sufficient insight in the self-organization process by discussing the role of the spectral transfer due to nonlinear couplings and the selective decay mechanism. A one-dimensional spectrum is obtained by considering the kinetic energy of the flow

$$E(x,y,t)=\sum_{n=0}^{N}\sum_{m=0}^{N}\hat{E}_{nm}(t)T_n(x)T_m(y), \tag{7}$$

along the lines $x=0$ and $y=0$. The one-dimensional spectrum $\hat{S}_n(t)$ is defined as an average of both contributions

$$\hat{S}_n(t)=\frac{1}{2}\left|\sum_{m=0}^{N}[\hat{E}_{nm}(t)+\hat{E}_{mn}(t)]T_m(0)\right|. \tag{8}$$

Note that $\hat{S}_n(t)$ is always positive by definition. Several spectra $\hat{S}_n(t)$, computed for the simulation with Re=2000 (see Fig. 1), are shown in Figs. 3(a)–3(d) (even Chebyshev coefficients) and Figs. 3(e)–3(h) (odd Chebyshev coefficients). Self-organization of the initially turbulent flow is clearly visible in the change of the distribution of excited Chebyshev modes: The high-frequency modes dissipate rather fast and this process outweighs turbulent spectral transfer from low to high Chebyshev modes (selective decay), and the increasing amplitude of some of the lowest Chebyshev modes in the spectrum during the initial stage of decay. This latter process is only due to transfer by nonlinear interactions.

The total kinetic energy E and the enstrophy Ω for the run shown in Fig. 1 are plotted in Fig. 4 as a function of time. The decay of enstrophy is much faster than the decay of energy as long as the flow is not completely determined by viscous effects. Diffusion of vorticity strongly dominates advection for eddy turnover times larger than 130 ($\approx 3\sqrt{\mathrm{Re}}$, see Sec. III B), as can be concluded by observing that the decay rates of E and Ω start to become equal for large times. Another interesting aspect is the decay of the angular momentum after spin-up has occurred ($t\cong 10$, see Fig. 2 upper curve). Two different regimes can be recognized: The intermediate stage of decay ($10\leqslant t\leqslant 80$) where the angular momentum is approximately constant, or at least nondecaying, and the final decay stage where the angular momentum decays roughly twice as slow as the kinetic energy (for a discussion of the final decay stage, see Sec. III C). Although the slow decay of L with respect to E was also observed for decaying 2D turbulent flows in circular domains,[23–25] it is somewhat surprising that a regime with an approximately nondecaying angular momentum (after spontaneous spin-up) is also observed so clearly for flows in square containers. Li *et al.* ascribed the slow decay of L for flows in circular containers to the fact that in a circular domain angular momentum is an inviscid constant of the motion. However, this is not the case in a square domain. The rather surprising observation of the slow decay of L is most likely related to a slow decay of the symmetric (with respect to $x=0$ and $y=0$) vorticity modes compared with the decay of the other vorticity modes. This decay scenario, which might be considered as an alternative selective decay mechanism, results in a growing dominance of symmetric modes over antisymmetric modes. This is reflected by the presence of angular momentum in the flow, because only symmetric modes contribute to L. Decomposition of the vorticity field in symmetric and antisymmetric modes in several runs for Re=1000 and 1500 confirms this selective decay mechanism. From these observations it might be concluded that a large amount of L during the intermediate decay stage actually announces the appearance of predominantly symmetric vortex flow in the container.

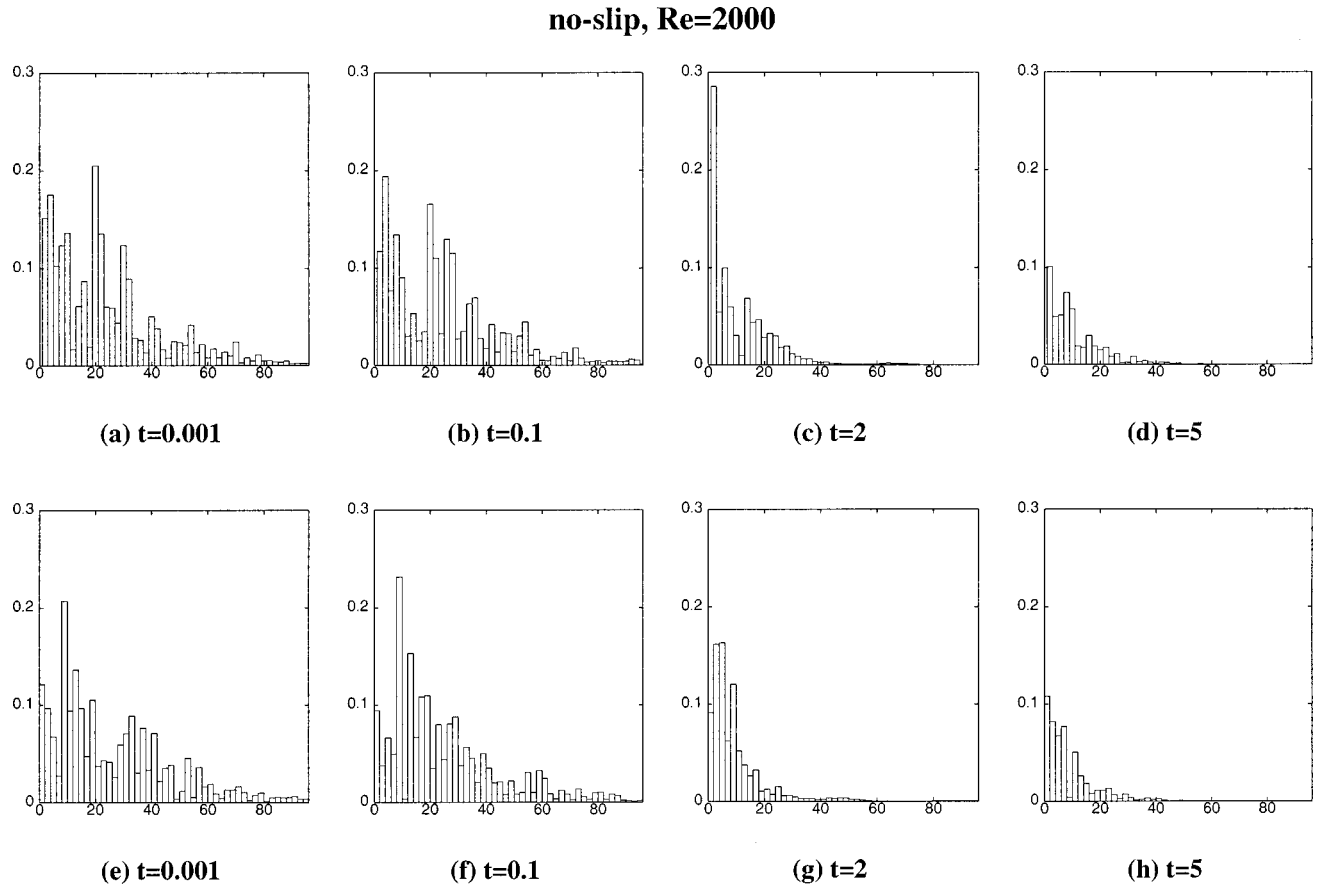

FIG. 3. One-dimensional Chebyshev spectrum $\hat{S}_n(t)$ of a simulation with no-slip boundary conditions, Re=2000. The spectra displayed in (a)–(d) represent even Chebyshev modes, while those in (e)–(h) represent odd Chebyshev modes.

B. Generalizations based on ensemble averaging

Some remarkable features of the flow evolution of decaying 2D turbulence in a square container with no-slip boundaries have been illustrated in the previous section. Several runs have been carried out for Re=1000, 1500, and 2000, and these were used to extract additional information such as characteristic time scales of freely decaying 2D turbulence, scaling behavior, and decay exponents of vortex density and vorticity extrema.

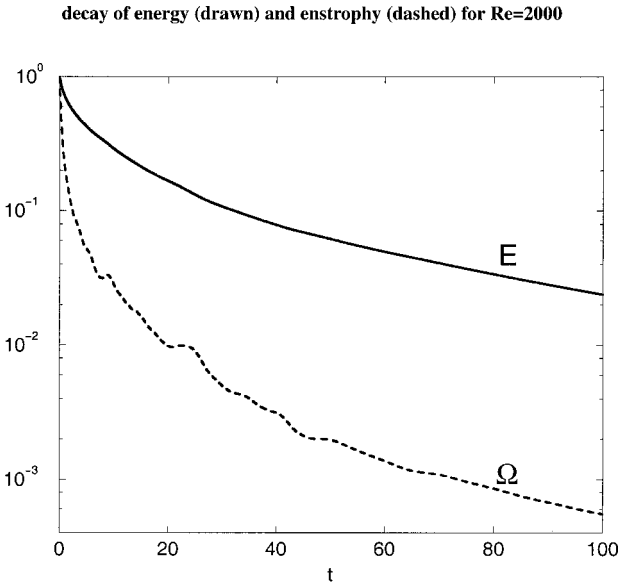

FIG. 4. The normalized energy, $E/E(t=0^+)$, and the normalized enstrophy, $\Omega/\Omega(t=0^+)$, plotted logarithmically vs dimensionless time t for Re =2000. The simulations are carried out with no-slip boundaries.

The importance of the presence of boundaries depends on the size of the container relative to the size of the dominant flow structures. This effect has been investigated by computing the ratio Ω/E, which can be interpreted as a mean-square wave number, i.e., $\Omega/E \sim \langle k^2 \rangle$. The decrease of Ω/E is indicative of the efficiency of the self-organization process. The relatively fast decay of Ω/E, due to turbulent spectral transfer and subsequent fast dissipation of high-frequency modes, is referred to in the literature as selective decay.[3] In Fig. 5(a) an ensemble-averaged value of the ratio $\Omega_{\mathrm{nor}}(t)/E(t)$, with $\Omega_{\mathrm{nor}}(t)=\Omega(t)/\Omega(t=0^+)$, is plotted as function of the dimensionless time. The ensemble average is based on twelve runs for each of the Reynolds numbers considered in this numerical investigation (Re=1000, 1500, and 2000). The algebraic decay rate for Ω_{nor}/E, which extends two to three decades, is remarkable and is found to be $\Omega_{\mathrm{nor}}/E \sim t^{-0.63}$. By introducing a new dimensionless time $T=t/\sqrt{\mathrm{Re}}$, the three ensemble averaged curves of Ω_{nor}/E are found to collapse onto a single curve, as is shown in Fig. 5(b). From this plot one can clearly identify the following characteristic times: $T \cong 1.7\times 10^{-2}$ as the time when Ω_{nor}/E

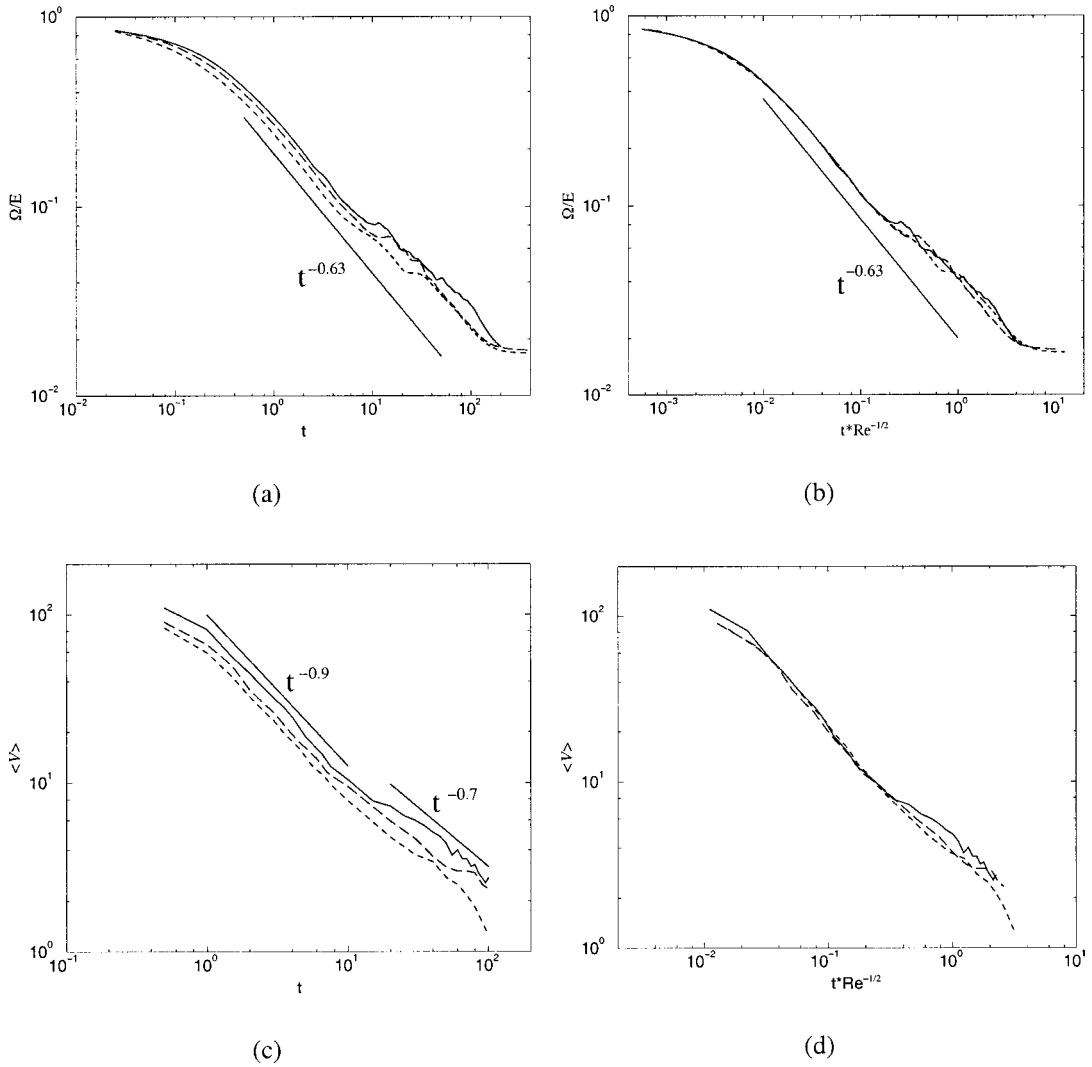

FIG. 5. The ratio Ω_{nor}/E plotted as function of t (a) and $T=t/\sqrt{\mathrm{Re}}$ (b), and the average number of vortices $V(t)$ plotted as function of t (c) and $T=t/\sqrt{\mathrm{Re}}$ (d). The data are based on ensemble averages of runs carried out for Re=1000 (short dashed), 1500 (dashed), and 2000 (drawn), respectively. Straight lines: $t^{-0.63}$ (a)–(b), $t^{-0.9}$ and $t^{-0.7}$ (c).

starts to decay algebraically, and $T\cong 0.2$ as the time at which vortex–wall interactions (and thus the presence of no-slip boundaries) become significant. The average size of the vortices has by then increased to $\lambda(T\cong 0.2)\cong 0.4W$, which can be inferred from Ω/E (without normalization of Ω) because $\lambda\cong 2\pi W\sqrt{E/\Omega}$. During the later stage it appears that Ω_{nor}/E again decays algebraically with $t^{-0.63}$. Finally, for $T\geqslant 6$ the kinetic energy and the enstrophy decay with the same rate, i.e., Ω_{nor}/E is constant, and the flow decays self-similarly (see Sec. III C). The characteristic size of the final vortex is then: $\lambda\cong 1.8W$. It is interesting to note that an ensemble average of Ω_{nor}/E has also been computed for the simulations with stress-free boundary conditions (sixteen runs with Re=2000). The algebraic decay is now found to be $\Omega_{\mathrm{nor}}/E\sim t^{-0.85}$, and the algebraic decay sets in later: At $T\cong 4.5\times 10^{-2}$ for the stress-free runs, compared with $T\cong 1.7\times 10^{-2}$ for the no-slip runs. This remarkable difference is entirely due to the presence of different boundary conditions.

The discussion of the ensemble average of Ω_{nor}/E reveals generalized time scales for the three characteristic stages of decaying 2D turbulence in containers with rigid no-slip walls (see discussion in Sec. III A). The initial stage takes place during the interval $0\leqslant t\leqslant 0.2\sqrt{\mathrm{Re}}$, the second stage (including spontaneous spin-up) for $0.2\sqrt{\mathrm{Re}}\leqslant t\leqslant 3\sqrt{\mathrm{Re}}$, and the third stage for $t\geqslant 3\sqrt{\mathrm{Re}}$, when the flow starts to become strongly diffusion dominated. This regime is characterized by a nearly exponential decay of both the energy and the enstrophy. The viscous decay regime, in which the flow is dominated by the slowest decaying viscous eigenmode (see Sec. III C), sets in for $t\geqslant 6\sqrt{\mathrm{Re}}$; the ratio Ω_{nor}/E is then constant.

The temporal evolution of decaying 2D turbulence during the initial decay stage is characterized by merging of vortices, and consequently the number of vortices, denoted by V, decreases. The role of the no-slip boundaries on the rate of decrease of V is not known yet. When, for example, a primary vortex approaches the boundary, a filament with oppositely signed vorticity is created. This boundary layer can roll up into a vorticity blob, thus actually increasing the num-

TABLE III. Power law exponents for decay rates of several quantities obtained from simulations with no-slip boundaries. The power laws of present results are expressed as: $f(t)\sim \mathrm{Re}^{\eta} t^{\xi}$. All decay exponents concern power laws for the initial turbulent decay regime. The decay exponents ξ_{car}, ξ_{dri}, and ξ_{exp} are the theoretical exponents (Ref. 30), the exponents obtained from a contour dynamics simulations of 2D turbulence on a sphere (Ref. 32), and some recent experimentally measured decay exponents (Ref. 33), respectively.

$f(t)$	ξ	η	ξ_{car} (Ref. 30)	ξ_{dri} (Ref. 32)	ξ_{exp} (Ref. 33)
$N(t)$	-0.90	0.5	-0.75	-0.29	-0.70
$a(t)$	$+0.31$	$\cdots$	$+0.19$	$+0.19$	$+0.21$
$\omega_{\mathrm{ext}}(t)/\sqrt{E(t)}$	-0.30	0.5	0	0	-0.09
$\Omega(t)/E(t)$	-0.63	$\cdots$	-0.38	-0.35	-0.18
$S_{\mathrm{ns}}(t)$	-0.42	0.0	$\cdots$	$\cdots$	$\cdots$
$F_{\mathrm{ns}}(t)$	-0.84	0.5	$\cdots$	$\cdots$	$\cdots$

ber of vortices. The strength of the primary vortex is usually strongly reduced by this vortex–wall interaction, and it might eventually be destroyed more rapidly by interaction with neighboring vortices, thus decreasing the number of vortices. One might not presume *a priori* that production and destruction of vortices due to flow–boundary interactions balance exactly. Recently, Carnevale *et al.*[30] proposed a scaling theory for freely decaying 2D turbulence in the limit $\mathrm{Re}\to\infty$ on an unbounded domain, based on the assumption that both the kinetic energy and the extremum of vorticity are conserved quantities during the decay process. Their approach results in algebraic decay of the number of vortices, i.e., $V(t)\sim t^{-\xi}$. The exponent ξ is so far undetermined, but has been found in both Navier–Stokes simulations and modified point-vortex methods to be $\xi\approx 0.70-0.75$.[30,31] Although the present simulations do not satisfy the conditions for freely decaying 2D turbulence in the infinite Reynolds number limit on an unbounded domain, it is still useful to consider the decay rate of $V(t)$, the average vortex radius $a(t)$, and the renormalized (by $\sqrt{E(t)}$) decay rate of the vorticity extremum of the dominant vortices. To determine these decay rates the computed curves for $V(t)$, $a(t)$, and $\omega_{\mathrm{ext}}(t)/\sqrt{E(t)}$ have been calculated for the runs with $\mathrm{Re}=1000$, 1500, and 2000, respectively.

Based on an ensemble average of the runs with $\mathrm{Re}=2000$ it was possible to find two decay exponents for the average vortex number: during the initial decay stage it is found that $V(t)\sim t^{-0.90\pm 0.03}$, and during the intermediate decay stage some evidence exists that $V(t)\sim t^{-0.7\pm 0.1}$ [see Fig. 5(c)]. In the initial stage, the average number of vortices decreases from approximately $V(t=1)\simeq 100$ to $V(t=10)\sim 10$ (with a standard deviation of approximately 8%, where the standard deviation is defined by $\sigma(t)=[(\langle V^2(t)\rangle - \langle V(t)\rangle^2)^{0.5}]/M$ with M the total number of simulations used in ensemble averaging), and in the intermediate decay stage, with decay exponent $\xi=0.7$, the average number of vortices decreases further to $V(t=100)\sim 2$ (with a standard deviation of roughly 15%). Although the standard deviation is relatively large, the decay exponent in the turbulent decay regime is rather robust. For example, all runs with $\mathrm{Re}=2000$ show the same decay exponent, viz. $V(t)=Ct^{-0.90}$, but a variation in the constant C is observed, thus resulting in a relatively large standard deviation. For $\mathrm{Re}=1000$ and 1500 the same decay exponents are found, although the regime in which $V(t)\sim t^{-0.7}$ is less clear [see Fig. 5(c)]. For convenience, all decay exponents of the initial turbulent regime are summarized in Table III, where also the theoretical results from Carnevale *et al.*,[30] some numerical results by Dritschel,[32] and some experimentally obtained decay exponents[33] are tabulated.

The power law for the average vortex radius is directly obtained from Ω/E by assuming $a(t)\sim\sqrt{E(t)/\Omega(t)}$, thus $a(t)\sim t^{0.31}$ (simulations with stress-free boundary conditions show a more rapidly increasing average vortex radius: $a(t)\sim t^{0.43}$).

The average decay rate of the renormalized vorticity extrema is found to be: $\omega_{\mathrm{ext}}(t)/\sqrt{E(t)}\sim t^{-0.30\pm 0.02}$. The ensemble-averaged curves computed for $\mathrm{Re}=1500$ and 2000 are displayed in Fig. 6. One can also observe that for $t\geqslant 40$ (for the runs with $\mathrm{Re}=2000$ and 1500) $\omega_{\mathrm{ext}}(t)/\sqrt{E(t)}$ is approximately constant ($\omega_{\mathrm{ext}}(t)/\sqrt{E(t)}\sim t^{-0.10\pm 0.04}$). Two more conclusions can be drawn: The ensemble averaged curves for both $V(t)$ and $\omega_{\mathrm{ext}}(t)/\sqrt{E(t)}$, for each Reynolds number considered in this study, are found to collapse onto a single curve by again using $T=t/\sqrt{\mathrm{Re}}$ as new dimensionless time [see Fig. 5(d) for $V(t)$], and it appears that during the initial decay stage ($0\leqslant t\leqslant 0.2\sqrt{\mathrm{Re}}$) the number of vortices is proportional with $\sqrt{\mathrm{Re}}$. Additionally, it is observed that the

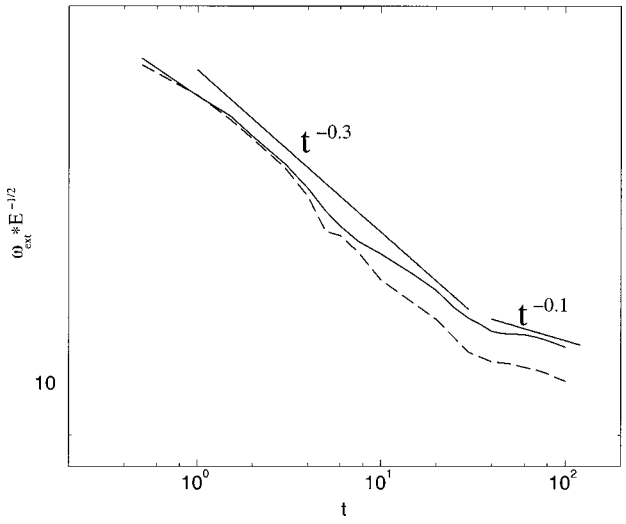

FIG. 6. The normalized vorticity extremum $\omega_{\mathrm{ext}}/\sqrt{E(t)}$ plotted as function of t. The data are based on ensemble averages of runs carried out for $\mathrm{Re}=1500$ (dashed) and 2000 (drawn), respectively. Straight lines: $t^{-0.3}$ and $t^{-0.1}$.

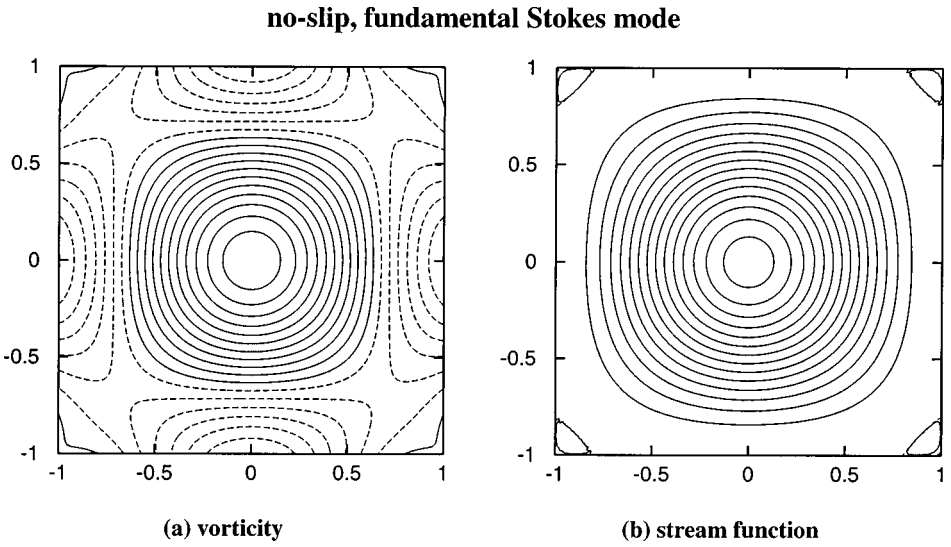

FIG. 7. Fundamental Stokes mode for flow on a square domain with no-slip boundaries: Contour plots of vorticity (a) and stream function (b).

power law behavior of $V(t)$ and $\omega_{\mathrm{ext}}(t)/\sqrt{E(t)}$ during the intermediate decay stage compare rather well with the experimentally measured decay exponents by Hansen, Marteau, and Tabeling:[33] $V(t)\sim t^{-0.70\pm0.1}$, and $\omega_{\mathrm{ext}}(t)/\sqrt{E(t)}\sim t^{-0.09\pm0.04}$.

Finally, the viscous stress and the amount of vorticity gradients near boundaries are calculated for the initial turbulent decay phase ($t\leqslant 0.2\sqrt{\mathrm{Re}}$). The magnitude of the viscous stress (nondimensionalized by ρU^2, with ρ the fluid density and U a characteristic velocity) at the boundary of the domain with no-slip walls is computed as follows, where we have used that the normal viscous stress is absent at no-slip walls since ($\nabla\cdot\mathbf{u}=0$):

$$\left[\int_{\partial D}\left(\frac{\partial u}{\partial n}\right)^2 ds\right]^{1/2}\Rightarrow\left[\int_{\partial D}\left(\frac{\partial u_{\parallel}}{\partial n}\right)^2 ds\right]^{1/2} \tag{9}$$

with $\partial/\partial n$ denoting the normal derivatives, ds the length of an infinitesimal element of the boundary ∂D, and $u_{\parallel}$ the velocity component parallel to the boundary. The numerical factor is due to normalization by the square root of the dimensionless length of the boundary. Note that the average viscous stress is equivalent to the average magnitude of the vorticity on the boundary. An interesting trend has been observed for the turbulent initial decay stage: $S_{\mathrm{ns}}(t)$ is approximately independent of the Reynolds number for $1000\leqslant \mathrm{Re}\leqslant 2000$. Furthermore, the following decay rate has been found for this decay regime: $S_{\mathrm{ns}}(t)\sim t^{-0.42\pm0.02}$ for $\mathrm{Re}=1000$, 1500, and 2000. The average of the vorticity gradient near the boundaries can be quantified by computing

$$F_{\mathrm{ns}}=\frac{1}{4}\sqrt{2}\,\mathrm{Re}^{-1}\left[\int_{\partial D}\left(\frac{\partial \omega}{\partial n}\right)^2 ds\right]^{1/2}. \tag{10}$$

The observed trend for the scaling behavior of this quantity appears to be: $F_{\mathrm{ns}}\sim\sqrt{\mathrm{Re}}$. Combination of both results confirms that the average boundary layer thickness δ scales like $\delta\sim W(S_{\mathrm{ns}}/F_{\mathrm{ns}})\sim W/\sqrt{\mathrm{Re}}$. The decay rate for $F_{\mathrm{ns}}(t)$ in the turbulent initial decay stage is: $F_{\mathrm{ns}}(t)\sim t^{-0.84\pm0.03}$. Combination of the power laws of $S_{\mathrm{ns}}(t)$ and $F_{\mathrm{ns}}(t)$ indicate that, during the initial turbulent decay stage, the boundary layer thickness grows like $\delta(t)\sim t^{0.4}$.

C. The viscous decay stage

The final decay stage of 2D turbulence in present simulations is characterized by a self-similar viscous decay of the fundamental mode of Stokes flow ($\mathrm{Re}=0$) on a square domain. The fundamental mode, as well as several higher modes, has been calculated analytically by Van de Konijnenberg *et al.*[9] Their analytical derivation and the numerical procedure to calculate the Stokes modes will not be reproduced in full length. Starting point is the vorticity equation on the square domain

$$\frac{\partial\omega}{\partial t}=\nu\nabla^2\omega, \tag{11}$$

with no-slip boundary conditions (note that no boundary conditions for the vorticity are available) and an initial condition $\omega_0\equiv\omega(x,y,t=0)$. The full time-dependent solution has the following form:

$$\omega(x,y,t)=\sum_{\mu} C_{\mu}\omega_{\mu}(x,y)e^{-\mu\nu t/W^2}, \tag{12}$$

where the constants C_{μ} are determined by the initial condition $\omega_0(x,y)$. Precise values of μ have to be determined yet. For each value of μ the following Helmholtz equation for $\omega_{\mu}(x,y)$ has to be solved:

$$\nabla^2\omega_{\mu}(x,y)+\frac{\mu}{W^2}\omega_{\mu}(x,y)=0, \tag{13}$$

with no-slip boundary condition at the rigid boundaries. In order to proceed it is necessary to consider Eq. (13) in terms of the stream function $\psi_{\mu}(x,y)$, which yields a fourth-order partial differential equation. The no-slip boundary condition can be reformulated in the necessary boundary conditions for the stream function, and a solution for the Stokes modes can, in principle, be determined. The vorticity and stream function corresponding to the fundamental Stokes mode, i.e., the mode with the smallest value of μ, are plotted in Figs. 7(a)

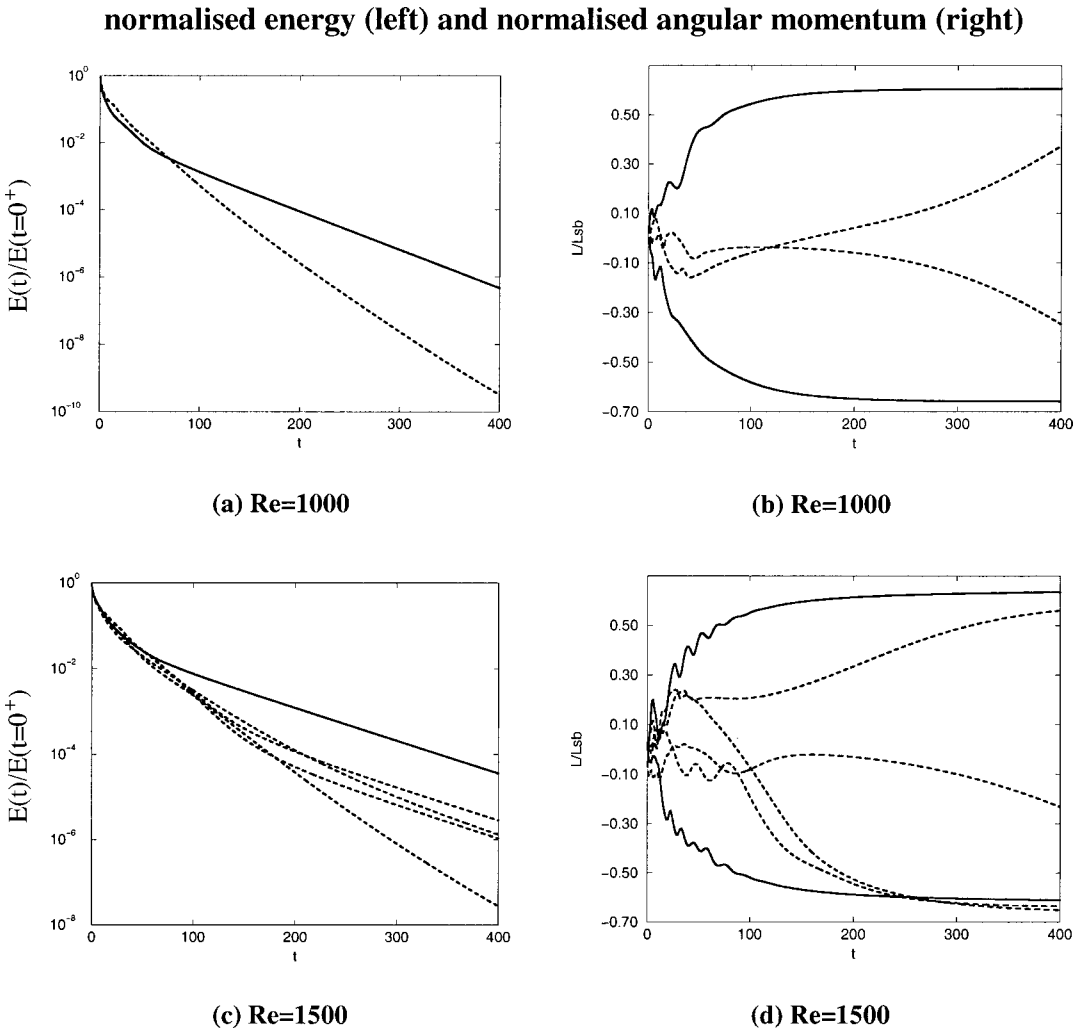

FIG. 8. The normalized energy, $E/E(t=0^+)$, and the normalized angular momentum, $L(t)/L_{sb}(t)$, are plotted vs dimensionless time t in order to compare different decay scenarios. The normalized energy for Re=1000 and 1500 is shown in (a) and (c), respectively. The normalized angular momentum is shown in (b) and (d) for Re=1000 and 1500, respectively. Note that less curves are drawn for the normalized energy in (a) and (c); some of the curves appeared to be hardly indistinguishable from each other.

and 7(b). The dimensionless eigenvalue for the fundamental mode is: $\mu=13.09$.

Long-time behavior of the kinetic energy, the enstrophy, and the total angular momentum, as observed in present numerical runs, can be understood by considering the decay of the fundamental Stokes mode

$$E(t)=\frac{1}{2}\int_D \mathbf{u}^2 dxdy \simeq e^{-2\mu\nu t/W^2}, \tag{14a}$$

$$\Omega(t)=\frac{1}{2}\int_D \omega^2 dxdy \simeq e^{-2\mu\nu t/W^2}, \tag{14b}$$

and

$$L(t)=\mathbf{k}\cdot\int_D \mathbf{r}\times\mathbf{u}\,dxdy \simeq e^{-\mu\nu t/W^2}, \tag{14c}$$

(with $\mu=13.09$). Computed decay rates of the kinetic energy and enstrophy in the final stage of 2D decaying turbulence are indeed the same, and the decay rate of the total angular momentum is twice as slow as that of the kinetic energy.

Several runs have been carried out (see Sec. III B) and for the viscous relaxation regime ($t\geqslant 3\sqrt{\mathrm{Re}}$) these runs can be subdivided into two groups. The majority (75%) shows mutually similar behavior with a rapid transition to the fundamental Stokes mode (a symmetric mode, see Fig. 7) in the final decay stage. All these runs show spontaneous spin-up. The other runs (25%), however, show anomalous behavior: A decaying antisymmetric mode is observed, and the transition to the fundamental Stokes mode occurs extremely slowly. These runs are characterized by the absence of spontaneous spin-up, or show only a weak spin-up behavior. From these results it is clear that presence or absence of spin-up of the flow can be associated directly with the appearance of symmetric or antisymmetric modes during the final decay stage, respectively, although spin-up of the flow occurs in the early stage of the decay of 2D turbulence. The normalized energy $E(t)/E(t=0^+)$ and the normalized total angular momentum $L(t)/L_{\mathrm{sb}}(t)$ [$L_{\mathrm{sb}}(t)$ is the angular momentum of the same amount of fluid with total kinetic energy $E(t)$, in solid body rotation] are plotted for several runs in Figs. 8(a) and 8(b) (Re=1000) and 8(c) and 8(d) (Re =1500). Dashed curves represent the anomalous runs; they

show a slow appearance the lowest Stokes eigenmode. The computed decay rates of the energy for the runs where the quasi-stationary final state is dominated by the lowest Stokes eigenmode are: $\mu(\mathrm{Re}=1000)=13.1\pm0.2$ and $\mu(\mathrm{Re}=1500)=13.2\pm0.2$. These results are close to the exact value $\mu=13.09$ as obtained by Van de Konijnenberg *et al.*[9]

IV. COMPARISON OF SIMULATIONS WITH NO-SLIP AND STRESS-FREE BOUNDARY CONDITIONS

A. General features of runs with stress-free boundary conditions

The dynamics of decaying 2D turbulence with stress-free boundary conditions is essentially different from that with no-slip boundary conditions, as shown in the simulations discussed in Sec. III. The initial stage of the flow is now characterized by the emergence of vortices with both positive and negative circulations, but they generally do not form many strong dipolar-like structures as usually observed during the initial stage of runs with no-slip boundary conditions. When no-slip boundaries are used, the emerging dipoles have a tendency to move to one of the boundaries and interact with it quite strongly. Simulations with stress-free boundary conditions reveal that the monopolar vortices tend to move parallel with the boundaries. Such behavior can be understood by realizing that a stress-free boundary acts as a mirror, and a vortex near the boundary observes a virtual vortex with opposite circulation at the other side of the boundary. Both vortices form a couple, and move parallel with the boundary. Another interesting difference between stress-free and no-slip simulations concerns the absence of vorticity filament production near the rigid walls in the stress-free case.

A remarkable feature of the flow dynamics in containers with stress-free boundary conditions is the *net leakage (diffusion) of vorticity* through the boundaries. This process is responsible for the change of total circulation Γ of the flow. Net leakage of vorticity through the boundaries is absent for flows in containers with no-slip boundaries, where $\Gamma=\int\omega dxdy\equiv0$, as well as for flows with periodic boundary conditions. In the latter case it is obvious that vorticity leaving the domain at one side is entering the domain at the other side; it is easy to verify from the definition of the circulation that in this case $\Gamma\equiv0$. The relation between the rate of change of circulation of the flow and the net flux of vorticity through the boundary of the domain, or, in the case of no-slip boundaries, the absence of a net leakage of vorticity is easily understood by considering the vorticity equation integrated over the flow domain

$$\int_D \frac{\partial\omega}{\partial t}dxdy+\int_D \mathbf{u}\cdot\nabla\omega dxdy$$

$$=\frac{d\Gamma}{dt}+\int_{\partial D}\mathbf{n}\cdot\mathbf{u}\omega ds=\nu\int_D\nabla^2\omega dxdy, \tag{15}$$

where $\mathbf{n}$ is the unit outward pointing vector normal to the boundary and ds denotes the length of an infinitesimal element of the boundary ∂D. The boundary integral of the nonlinear term is always zero, because either $\mathbf{u}=0$ (no-slip) or $\omega=0$ (stress-free) on the boundary. The rhs of Eq. (15) can also be reformulated in terms of a boundary integral, and finally a relation between the rate of change of circulation and the net vorticity flux through the boundary ∂D is found

$$\frac{d\Gamma}{dt}=\nu\int_{\partial D}\mathbf{n}\cdot\nabla\omega ds. \tag{16}$$

For no-slip boundary conditions $\Gamma\equiv0$, implying that the net vorticity flux through the boundary is also zero.

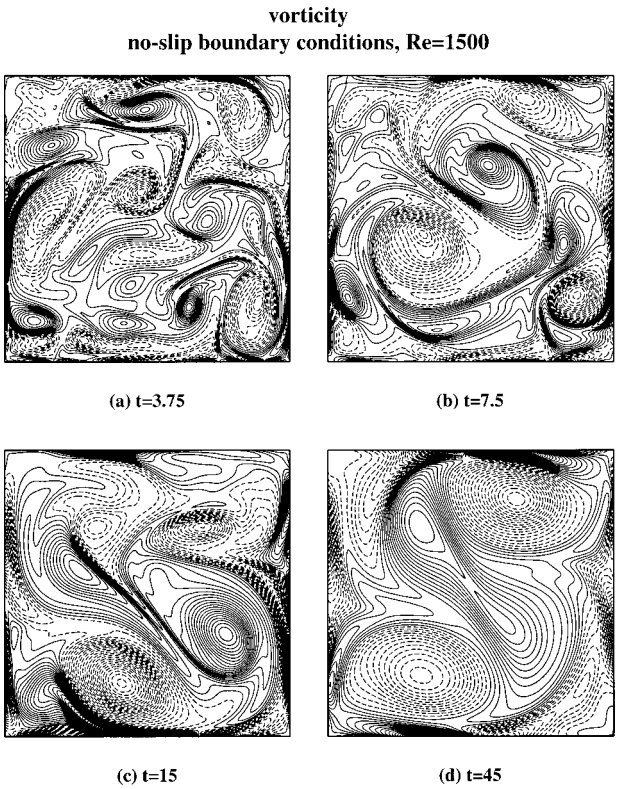

FIG. 9. Vorticity contour plots of a simulation with no-slip boundary conditions, Re=1500. Dashed contours represent negative vorticity, and drawn contours represent positive vorticity. The contour level increment is: (a) 1, (b) 0.5, (c) 0.25, and (d) 0.1.

B. Decaying 2D turbulence with no-slip or stress-free boundary conditions; Re=1500

The dramatic differences in the flow evolution of decaying 2D turbulence with no-slip and stress-free boundary conditions are clearly demonstrated in Figs. 9 and 10, which show some snapshots of the vorticity (Fig. 9 for the no-slip run and Fig. 10 for the stress-free run) for simulations with Re=1500. Snapshots of $\omega(x,y)$ are shown for $t=3.75$, 7.5, 15, and 45. Drawn lines represent positive vorticity values and dashed lines negative ones. The no-slip run for Re=1500 is characterized by the formation of a large tripolar structure [see Fig. 9(d)], which survives up to $t\cong75$, although it decays slowly due to shear and to viscous dissipation of the satellites. The long-time decay process is characterized by the appearance of a slightly elliptic vortex in the center of the tank ($t\cong125$). This elliptic vortex rotates slowly and is surrounded by a ring of opposite vorticity. This structure finally relaxes to the lowest Stokes eigenmode solution, which was discussed in Sec. III C. In the case of

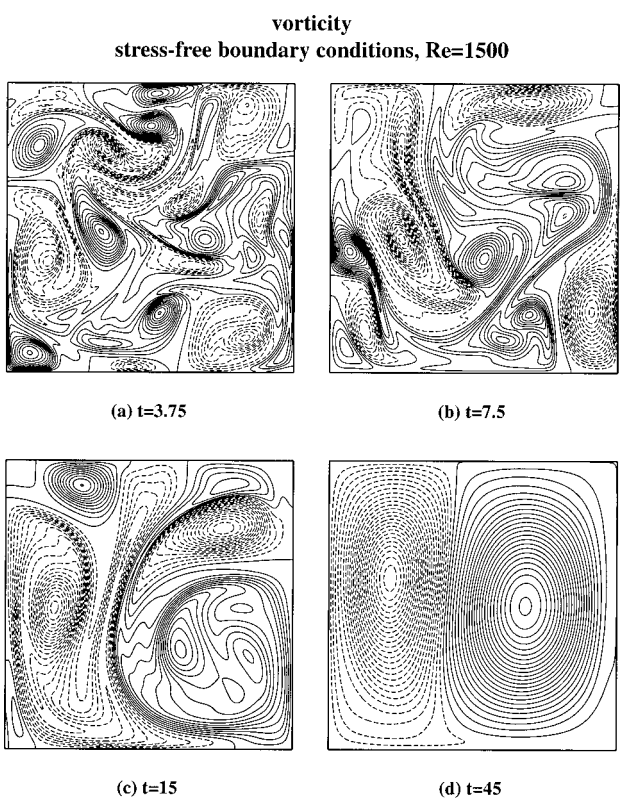

FIG. 10. Vorticity contour plots of a simulation with stress-free boundary conditions, Re=1500. Dashed contours represent negative vorticity, and drawn contours represent positive vorticity. The contour level increment is: (a) 1, (b) 0.5, (c) 0.25, and (d) 0.1.

stress-free boundary conditions the flow evolution is characterized by the formation of two large cells with opposite circulation, i.e., a large dipole. This dipole is observed to show a slow rotation in the container. During the final stage of decay of this stress-free run the vortex with negative circulation finally disappears due to a combination of dissipation and net leakage of vorticity through the boundaries of the container. This final state (a ''square'' domain-filling vortex with one sign of vorticity) compares rather well with the lowest eigenmode solution as calculated by Kondoh *et al.*[21] Similar scenarios have been observed for the stress-free runs with Re=1000 and 2000, and from a series of simulations with Re=2000 it can be conjectured that the formation of a rotating dipole during the intermediate stage of the decay process occurs most frequently; only a small minority of those runs revealed the rapid formation of a monopole during the intermediate decay stage.

Energy and enstrophy, computed for the no-slip and stress-free simulation with Re=1500, are plotted as function of dimensionless time in Figs. 11(a) (energy) and 11(b) (enstrophy). An important difference between the no-slip and stress-free results for E and Ω is easily observed: The decay of the energy and enstrophy in the stress-free run is an order of magnitude smaller than in the no-slip case. In the intermediate stage of the flow evolution it appears that self-organization sets in more rapidly in the numerical experiments with stress-free boundary conditions than in the no-slip case. This property is illustrated in Fig. 12, which shows

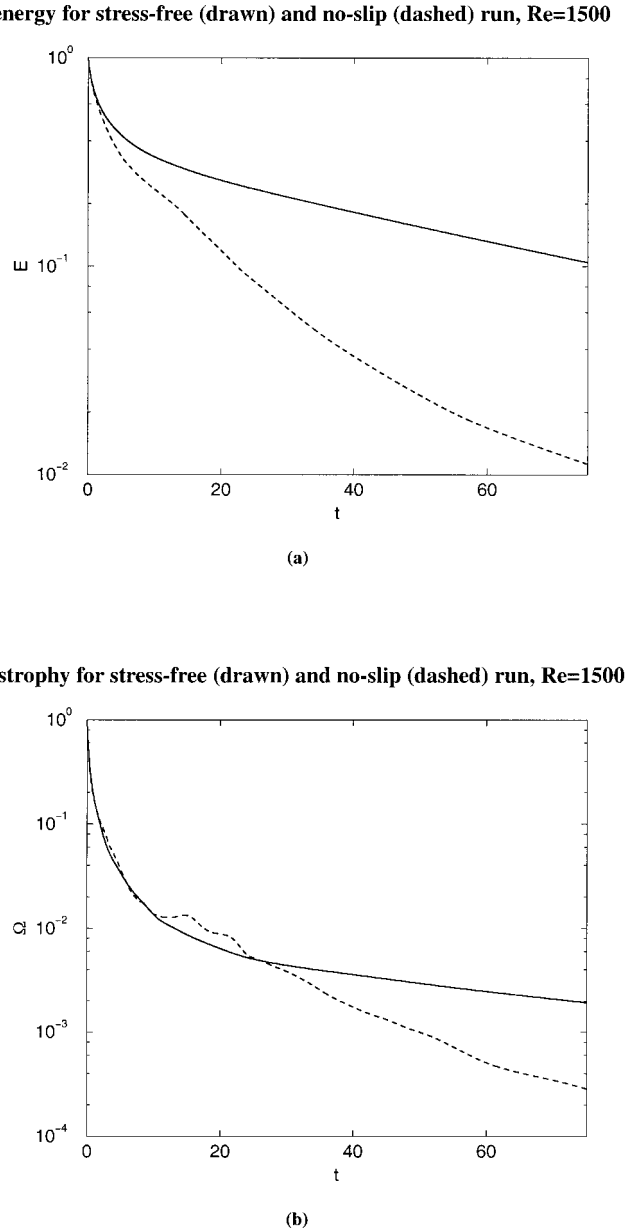

FIG. 11. The normalized energy, $E/E(t=0^+)$, and the normalized enstrophy, $\Omega/\Omega(t=0^+)$, plotted logarithmically vs dimensionless time t for Re =1500 in (a) and (b), respectively. The simulations are carried out with stress-free boundaries (drawn) and with no-slip boundaries (dashed).

plots of the ratio Ω/E, the mean-square wave number (see Sec. III B), as a function of the dimensionless time for the no-slip and the stress-free simulations, both for Re=1000 and for 1500. The curves in Fig. 12 show that a significant difference in scales occurs for $t \geqslant 8$ (comparable with $t = 0.2\sqrt{\mathrm{Re}}$) between the simulations with no-slip and stress-free boundaries. Also the presence of active boundary layers for the no-slip case is clear: Ω/E does not decrease monotonically as is the case for the run with stress-free boundaries. The average scale, estimated from $\Omega/E \sim \langle k^2 \rangle$, during the later stage of the flow evolution is approximately $\lambda(t = 50) \cong 1.2W$ for the no-slip runs, and $\lambda(t=50) \cong 1.8W$ for the stress-free case. Note that the simulations with no-slip boundaries show such large-scale structures ($\lambda \cong 1.8W$) for $t \geqslant 6\sqrt{\mathrm{Re}}$.

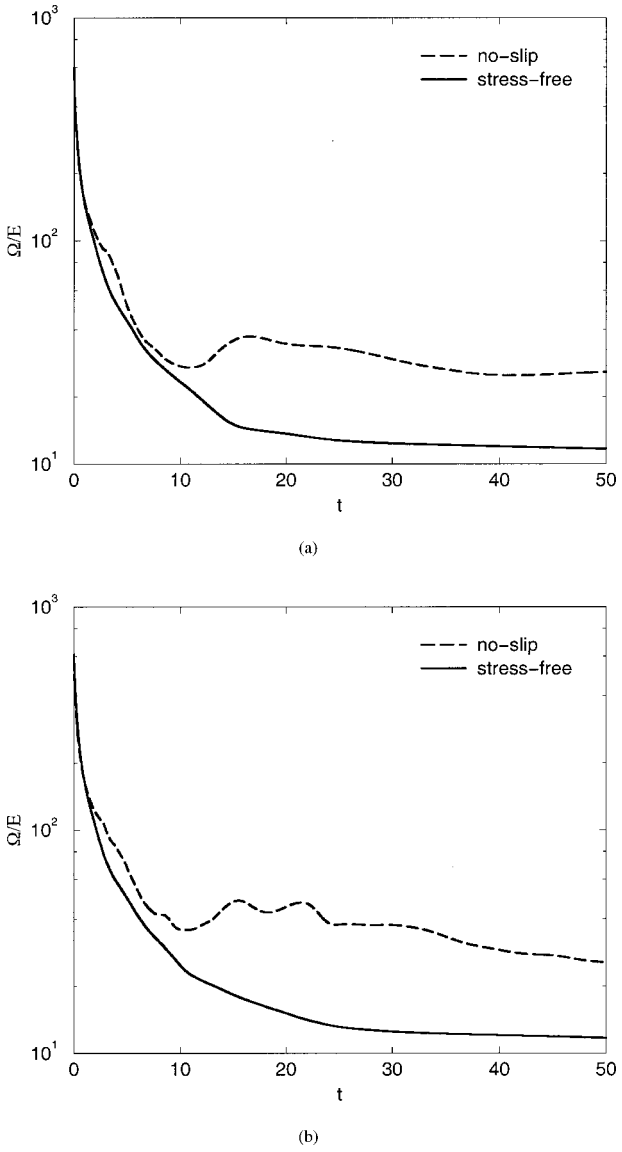

FIG. 12. The ratio Ω/E plotted vs dimensionless time for Re=1000 (a) and Re=1500 (b). The dashed and drawn lines represent results from simulations with no-slip and stress-free boundary conditions, respectively.

The scale difference observed in these numerical runs, and the faster decay of energy and enstrophy during the decay of 2D turbulence in the no-slip run compared with the decay observed in the stress-free run, can partly be understood with the selective decay hypothesis. Turbulent spectral transfer results in an accumulation at low Chebyshev modes, but also in an excitation of high Chebyshev modes representing small scales. Due to the presence of no-slip boundaries, even more small scales are produced in these runs than in the runs with stress-free boundaries (compare, e.g., Figs. 9 and 10). The resulting high Chebyshev modes decay rapidly and, obviously, the decay of energy and enstrophy during the decay of 2D turbulence should be larger for the no-slip runs than for the stress-free simulations. Note that the final decay is mainly determined by decaying low Reynolds number flow, as discussed in Sec. III C, and spectral transfer is almost absent. Consequently, E, Ω, and L decay according to the fundamental Stokes eigenmode solution which has different decay rates for either no-slip or stress-free boundaries. Additionally, net leakage of vorticity through the stress-free boundaries, as discussed in Sec. IV A, contributes to the more rapid self-organization in the stress-free runs and to the increased scale difference between the large-scale structures observed in no-slip and stress-free runs, respectively. This is due to the fact that small-scale vorticity patches near the stress-free boundary leak out of the domain, which induces symmetry breaking, and finally the appearance of a container-filling cell with one sign of vorticity.

It is also interesting to consider the so-called Weiss function Q[4,34] which is defined as

$$Q = S^2 - \omega^2 = \left(\frac{\partial u}{\partial x} - \frac{\partial v}{\partial y}\right)^2 + \left(\frac{\partial v}{\partial x} + \frac{\partial u}{\partial y}\right)^2 - \left(\frac{\partial v}{\partial x} - \frac{\partial u}{\partial y}\right)^2, \quad (17)$$

with S a measure of the rate of strain, $S^2 = -\det(\nabla \mathbf{u} + \nabla \mathbf{u}^T)$. Regions with negative Q are rotation-dominated ($\omega > S$) and are found in the vortex cores. These regions have an elliptic character (sometimes called neutral[4]), i.e., two fluid particles initially near each other in an elliptic region will stay close together. In regions where Q is positive the flow is strain-dominated ($S > \omega$) and has a hyperbolic character or, following McWilliams,[4] these regions have a turbulent nature. The distance between two fluid particles in a hyperbolic region will increase exponentially in time. Figs. 13 and 14 present contour plots of the Weiss function of simulations for Re=1500 with no-slip and stress-free boundary conditions, respectively. Snapshots of Q are shown for $t = 3.75$, 7.5, 15, and 45. Dashed contours represent hyperbolic regions ($Q > 0$), and elliptic regions are denoted by drawn contours ($Q < 0$). A comparison of Figs. 9(b) and 13(b) and Figs. 10(b) and 14(b) provides a clear example that illustrates the different dynamical behavior of the flow near no-slip and stress-free boundaries, respectively. Boundary layers in simulations with no-slip boundary conditions are always found in strain-dominated regions, which explains boundary layer detachment and elongation of vorticity filaments. The dynamics near stress-free boundaries is rather different, as can be observed in Fig. 10. In Fig. 10(b) two vortices with negative circulation are moving along the boundary; one is moving in the clockwise direction to the upper right corner and the other, moving in the same direction, to the lower right corner. Due to both the interaction with their respective images and with vortices in the interior these two negative vortices are squeezed, and vorticity gradients near the boundary steepen. In Fig. 14(b) it is observed that these regions are always situated in rotation-dominated ($Q < 0$) regions or in regions where strain only slightly dominates rotation. As a result, production of vorticity filaments is absent.

A remarkable difference between the Weiss function for flows with no-slip and with stress-free boundary conditions is the form of the regions with $Q < 0$ and $Q > 0$. When no-slip boundaries are used (see Fig. 13) it appears that during the decay stage the rotation-dominated regions have a circular or elliptical form and the remaining part of the flow domain is strain dominated. In the final decay stage, a large monopolar vortex is formed, and the accompanying Weiss

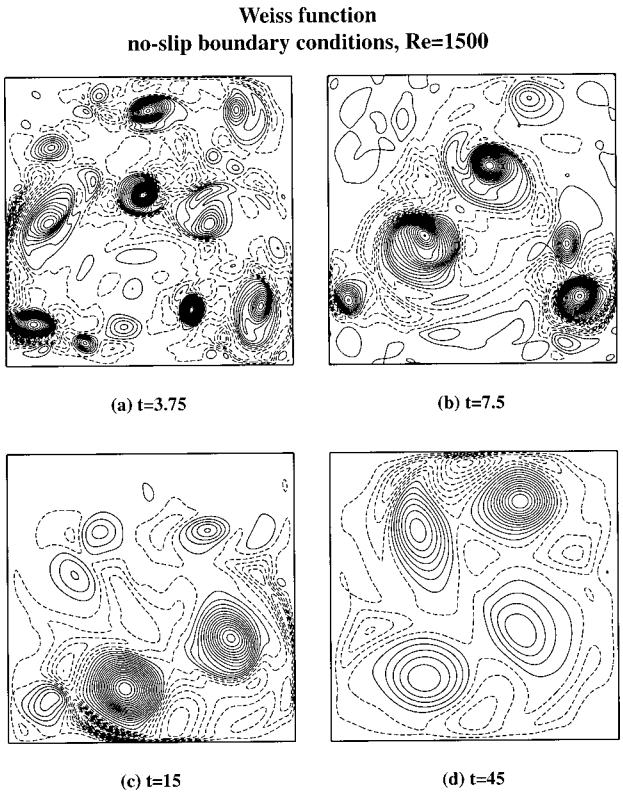

FIG. 13. Contour plots of the Weiss function (Q) of a simulation with no-slip boundary conditions, Re=1500 (see also Figs. 9 and 11). Dashed contours represent positive values of Q (hyperbolic regions), and drawn contours represent negative values (elliptic regions). The contour level increment is: (a) 10, (b) 4, (c) 2, and (d) 0.25.

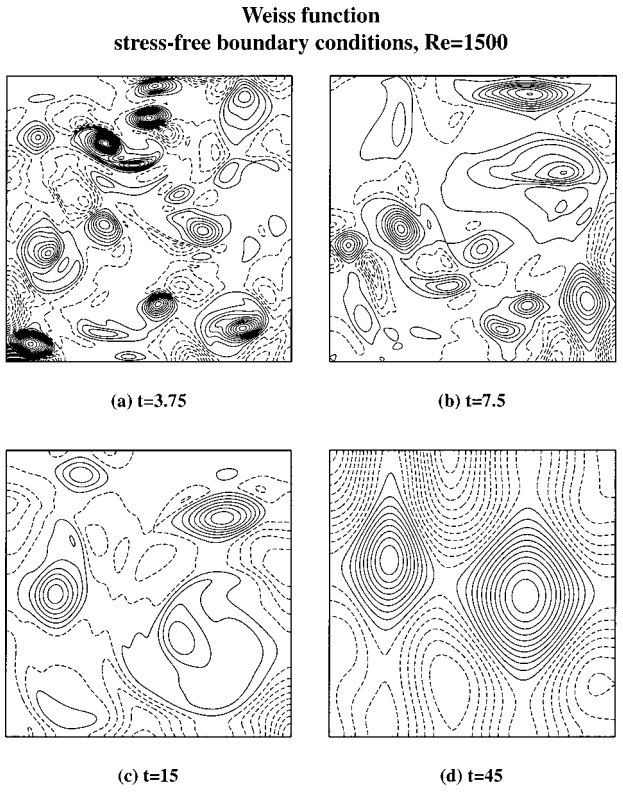

FIG. 14. Contour plots of the Weiss function (Q) of a simulation with stress-free boundary conditions, Re=1500 (see also Figs. 10 and 12). Dashed contours represent positive values of Q (hyperbolic regions), and drawn contours represent negative values (elliptic regions). The contour level increment is: (a) 10, (b) 4, (c) 2, and (d) 0.25.

function is a large circular rotation-dominated region in the center of the container surrounded by a ring where strain dominates. Applying stress-free boundary conditions (see Fig. 14) results always, thus also in the final decay stage, in lozenge-shaped regions with either rotation- or strain-dominated character. The contour plots shown in Figs. 13 and 14 are aimed at comparing the Weiss function for the no-slip and stress-free run at the same dimensionless times. This choice is based on the initial average eddy turnover time, which is equal for both runs in the initial decay stage ($t \leqslant 1$). An alternative approach, comparing the Weiss function for both boundary conditions at times at which the total kinetic energy of the flow [thus Re(t)] is the same for both runs, confirms our conclusion.

The magnitude of the dimensionless normal viscous stress for the stress-free case is computed as follows:

$$\left[\int_{\partial D}\left(\frac{\partial u}{\partial s}\right)^2 ds\right]^{1/2} \Rightarrow \left[\int_{\partial D}\left(\frac{\partial u_{\parallel}}{\partial s}\right)^2 ds\right]^{1/2} \tag{18}$$

with $\partial/\partial s$ denoting the tangential derivatives, and ds the length of an infinitesimal element of the boundary ∂D. Note that $|\partial u_1/\partial n| = |\partial u_{\parallel}/\partial s|$ at the boundary with $u_{\perp}$ the velocity component perpendicular to the boundary. Two interesting trends have been observed for the turbulent initial decay stage. In the first place, calculations show that S_{ns} (see Sec. III) is roughly an order of magnitude larger than S_{sf} (for $1000 \leqslant \mathrm{Re} \leqslant 2000$), thus viscous stresses are more intense near no-slip walls than near stress-free boundaries. In the second place, some amount of scaling has been observed for the magnitude of viscous stresses near the boundaries: S_{ns} is approximately independent from the Reynolds number, and $S_{\mathrm{sf}} \sim \mathrm{Re}^{-0.25}$. Leakage of vorticity through stress-free boundaries can be quantified by computing

$$F_{\mathrm{sf}} = \frac{1}{4}\sqrt{2}\,\mathrm{Re}^{-1}\left[\int_{\partial D}\left(\frac{\partial \omega}{\partial n}\right)^2 ds\right]^{1/2}, \tag{19}$$

which is a measure of the dimensionless vorticity flux through the boundaries. The observed trend for the leakage of vorticity is that F_{sf} is independent of the Reynolds number (in the turbulent regime). A kind of ''boundary layer thickness'' can be introduced for the stress-free case: $\delta_{\mathrm{sf}} \sim W(S_{\mathrm{sf}}/F_{\mathrm{sf}}) \sim W\,\mathrm{Re}^{-0.25}$. The behavior of S_{sf} and F_{sf} should be investigated in more detail, which will require more simulations for accurate ensemble averaging, particularly for higher Reynolds numbers before definitive conclusions can be drawn.

V. CONCLUSIONS

We have reported results of direct numerical simulations of decaying 2D turbulence inside a square container with rigid boundaries for several Reynolds numbers. From this investigation it is clear that the decay scenario of 2D turbulence is strongly modified by the presence of either no-slip or stress-free boundary conditions, and differs completely from

decaying 2D turbulence on a domain with periodic boundary conditions. Results of the latter simulations are frequently reported in the literature. Simulations with no-slip boundary conditions show that boundary layers play an important role in the decay of turbulence. The boundary layers serve as sources of small-scale vorticity, which is continuously injected into the interior of the flow domain, as these layers are generally formed in strain-dominated regions of the flow. Due to this process a rapid self-organization of the flow towards one or two large vortices is inhibited in the early stage of decaying turbulence. The role of the boundary layers gradually diminishes when the total energy of the flow decreases, and in a later stage of the flow evolution large vortices arise with size comparable with the container dimension. During the final stage of the flow evolution, the flow decays self-similarly according to the slowest decaying Stokes eigenmode of the vorticity diffusion equation. It is found, by considering an ensemble average of Ω/E, that the decay of 2D turbulence in a square container with no-slip boundaries consists of three generalized regimes (for Re $\leqslant$2000): The initial stage for $0 \leqslant t \leqslant 0.2\sqrt{\mathrm{Re}}$, the second stage (including spontaneous spin-up) for $0.2\sqrt{\mathrm{Re}} \leqslant t \leqslant 3\sqrt{\mathrm{Re}}$, and the final stage for $t \geqslant 3\sqrt{\mathrm{Re}}$ when the flow starts to become diffusion dominated. Viscous decay dominated by the slowest decaying viscous eigenmode sets in for $t \geqslant 6\sqrt{\mathrm{Re}}$. Simulations with stress-free boundary conditions show a much more rapid self-organization of the flow and also a relaxation to a slowest decaying Stokes eigenmode, satisfying $\omega = 0$ on the boundary, of the vorticity equation. The reason for the rapid self-organization is partly due to a less intense production of small scales near the boundary of the domain in comparison with simulations with no-slip boundary conditions. Another contribution is the net leakage of vorticity through stress-free boundaries, generally resulting in decreasing strength of (small-scale) structures near the boundary. Net leakage of vorticity is absent when no-slip boundaries are present. Additionally, the flow dynamics during the intermediate decay stage is substantially different for the two types of boundary conditions. This is, for example, illustrated with the plots of Ω/E in Figs. 5 and 12, which show enstrophy production in boundary layers near no-slip boundaries, and a different algebraic decay of Ω_{nor}/E ($\Omega_{\mathrm{nor}}/E \sim t^{-0.63}$ for no-slip simulations and $\Omega_{\mathrm{nor}}/E \sim t^{-0.85}$ for stress-free runs).

An interesting observation is the behavior of the total angular momentum (L) of the flow. The initial condition contains only a small amount of net angular momentum due to a zero-mean Gaussian random realization of the spectral coefficients of the initial velocity field. Very rapidly the total angular momentum of the flow increases to a considerably larger value due to spontaneous spin-up of the flow, and during the intermediate stage L remains approximately constant or decays only very slowly, while the decay of the total kinetic energy of the flow is considerable, regardless of the presence of no-slip or stress-free boundaries. The final (long-time) decay of L is governed by self-similar decay (as discussed, for example, in Sec. III C for runs with no-slip boundary conditions). Initial growth of L in simulations of flows on a square domain is due to turbulent spectral transfer combined with a selective decay mechanism, resulting in an increasing dominance of symmetric vorticity modes. It appears that the behavior of L in decaying turbulence on a square domain is intimately linked with the symmetry of the ''final'' state.

Scaling behavior for the number of vortices $V(t)$, the normalized vorticity extremum $\omega_{\mathrm{ext}}(t)/\sqrt{E(t)}$, the average vortex radius $a(t)$, and $\Omega_{\mathrm{nor}}(t)/E(t)$ are computed for the simulations with no-slip boundaries (see Table III). The difference of the temporal evolution with scaling theory is not completely surprising, since the present simulations are far from the infinite Reynolds number limit. Nevertheless, a further study seems worthwhile because simply applying different boundary conditions yields different scaling behavior (viz. no-slip versus stress-free). Additionally, the present simulations are initialized with a vortex population with a wide distribution of sizes, so a direct comparison with a few experimental studies of scaling properties of decaying 2D turbulence, based on a narrow distribution of vortex sizes for the initial flow field, is not possible yet (see, e.g., Tabeling *et al.*[12]). A more detailed comparison of vortex statistics in freely evolving 2D turbulence at higher Reynolds numbers (up to Re$\cong$10.000) in containers with no-slip walls and in domains with periodic boundary conditions is in preparation.

Recent theoretical, numerical, and experimental studies on 2D decaying turbulence were often based on the assumption that the decay could be assessed on the basis of statistical approaches, including maximum entropy theories[14–20] and the selective decay hypothesis,[3] and scaling theory.[30,31] Experimental studies by Marteau *et al.*[13] and numerical investigations by Jüttner *et al.*[22] were aimed at clarifying the relation between experimentally measured final states of decaying 2D turbulence and equilibrium states based on theoretical models. The experimental results[13] seem to support the scaling theory approach in favor of the computed equilibrium states based on a maximum entropy theory. The numerical investigations by Jüttner *et al.*[22] partly confirm the experimental results, but numerical simulations using the experimental data from Ref. 13 as artificial initial conditions (with stress-free boundary conditions) lead to somewhat different conclusions. When linear bottom friction (see for explanation Ref. 13) is used no equilibrium states are found, but when no linear bottom friction is used it appears that the final equilibrium states resemble the final states from the maximum entropy theory. This latter kind of simulations is equivalent with simulations of 2D decaying turbulence in a container with stress-free boundaries. From our results we can conclude that every analogy between final states of 2D decaying turbulence in containers with no-slip boundaries and final states predicted by maximum entropy theories is, however, accidental for the Reynolds numbers considered in this study. The observed decay towards final states, as found in 36 runs with $1000 \leqslant \mathrm{Re} \leqslant 2000$, is merely a relaxation to the slowest decaying Stokes eigenmode solution of the vorticity equation. Final states obtained from maximum entropy theories, although they do not represent inviscid flows due to coarse graining of the flow, represent flows for which the Reynolds number is still very large. It is still an open ques-

tion whether maximum entropy theories or other statistical approaches can be used to predict the intermediate state arising in simulations with significantly higher Reynolds numbers than used in the present investigation. Also, the assumption to approximate the rigid boundaries as present in experiments by stress-free boundary conditions in numerical simulations is incorrect, as can be concluded from the different decay scenarios for no-slip versus stress-free runs shown in Secs. III and IV. The other theoretical approaches, i.e., application of the selective decay hypothesis and the scaling theory, are worthwhile under the restriction that two different decay stages are recognized: Turbulent decay with spectral transfer and selective decay, and finally a decay stage in which diffusion dominates over nonlinear advection, i.e., spectral transfer is then absent in favor of self-similar decay.

Finally, the main conclusions, which are all based on ensemble averaging of 36 runs for $1000 \leqslant \mathrm{Re} \leqslant 2000$, are summarized. Freely evolving 2D turbulence in containers with no-slip boundaries consists of three characteristic stages: The turbulent initial stage, the spontaneous spin-up stage, and a final stage where the flow is characterized by viscous relaxation. A large majority of the runs (75%) show spontaneous spin-up of the flow (see Table II). During the initial turbulent decay regime ($0 \leqslant t \leqslant 0.2\sqrt{\mathrm{Re}}$) the average boundary layer thickness scales as $\delta \sim W/\sqrt{\mathrm{Re}}$, and the growth of the boundary layer thickness shows power-law behavior ($\delta \sim t^{0.4}$). The vortex radius is approximately a tenth of the container width at the moment ($t \sim 0.2\sqrt{\mathrm{Re}}$) when vortex–wall interactions start to dominate the flow evolution. Two power-law regimes with different decay behavior can be recognized for the vortex number and vorticity extremum (see Figs. 5 and 6): The initial turbulent regime, where the decay exponents are independent of Re and the intermediate decay stage where viscous effects influences the decay exponents. A comparison between simulations with no-slip and with stress-free boundary conditions shows a completely different behavior of freely decaying 2D turbulence.

ACKNOWLEDGMENTS

The authors gratefully acknowledge Professor David Montgomery (Dartmouth College, U.S.A.) and Dr. Anders Nielsen (RISØ, Denmark) for a number of useful discussions. One of us (S.R.M.) is grateful for support by the Netherlands Geosciences Foundation (GOA) with financial aid from the Netherlands Organisation for Scientific Research (NWO).

[1] M. E. Brachet, M. Meneguzzi, and P. L. Sulem, ''Small-scale dynamics of high-Reynolds number two-dimensional turbulence,'' Phys. Rev. Lett. **57**, 683 (1986).
[2] M. E. Brachet, M. Meneguzzi, H. Politano, and P. L. Sulem, ''The dynamics of freely decaying two-dimensional turbulence,'' J. Fluid Mech. **194**, 333 (1988).
[3] W. H. Matthaeus and D. Montgomery, ''Selective decay hypothesis at high mechanical and magnetic Reynolds numbers,'' Ann. (N.Y.) Acad. Sci. **357**, 203 (1980).
[4] J. C. McWilliams, ''The emergence of isolated coherent vortices in turbulent flow,'' J. Fluid Mech. **146**, 21 (1984).
[5] P. Santangelo, R. Benzi, and B. Legras, ''The generation of vortices in high-resolution, two-dimensional, decaying turbulence and the influence of initial conditions on the breaking of self-similarity,'' Phys. Fluids A **1**, 1027 (1989).
[6] W. H. Matthaeus, W. T. Stribling, D. Martinez, S. Oughton, and D. Montgomery, ''Decaying, two-dimensional, Navier–Stokes turbulence at very long times,'' Physica D **51**, 531 (1991).
[7] E. J. Hopfinger and G. J. F. van Heijst, ''Vortices in rotating fluids,'' Annu. Rev. Fluid Mech. **25**, 241 (1993).
[8] J. B. Flór, ''Coherent Vortex Structures in Stratified Fluids,'' Ph.D. thesis, Eindhoven University of Technology, The Netherlands (1994).
[9] J. A. van de Konijnenberg, J. B. Flór, and G. J. F. van Heijst, ''Decaying quasi-two-dimensional flow on a square domain,'' Phys. Fluids **10**, 595 (1998).
[10] B. M. Boubnov, S. B. Dalziel, and P. F. Linden, ''Source-sink turbulence in a stratified fluid,'' J. Fluid Mech. **261**, 273 (1994).
[11] J. M. Nguyen Duc and J. Sommeria, ''Experimental characterization of steady two-dimensional vortex couples,'' J. Fluid Mech. **192**, 175 (1988).
[12] P. Tabeling, S. Burkhart, O. Cardoso, and H. Willaime, ''Experimental study of freely decaying two-dimensional turbulence,'' Phys. Rev. Lett. **67**, 3772 (1991).
[13] D. Marteau, O. Cardoso, and P. Tabeling, ''Equilibrium states of 2D turbulence: an experimental study,'' Phys. Rev. E **51**, 5124 (1995).
[14] Y. B. Pointin and T. S. Lundgren, ''Statistical mechanics of two-dimensional vortices in a bounded container,'' Phys. Fluids **19**, 1459 (1976).
[15] P. H. Chavanis and J. Sommeria, ''Classification of self-organized structures in two-dimensional turbulence: the case of a bounded domain,'' J. Fluid Mech. **314**, 267 (1996).
[16] J. Miller, ''Statistical mechanics of Euler equations in two dimensions,'' Phys. Rev. Lett. **65**, 2137 (1990).
[17] R. Robert and J. Sommeria, ''Statistical equilibrium states for two-dimensional flows,'' J. Fluid Mech. **229**, 291 (1991).
[18] G. Joyce and D. Montgomery, ''Negative temperature states for the two-dimensional guiding centre plasma,'' J. Plasma Phys. **10**, 107 (1973).
[19] D. Montgomery, W. H. Matthaeus, W. T. Stribling, D. Martinez, and S. Oughton, ''Relaxation in two dimensions and the ''sinh-Poisson'' equation,'' Phys. Fluids A **4**, 3 (1992).
[20] D. Montgomery, X. Shan, and W. H. Matthaeus, ''Navier-Stokes relaxation to sinh-Poisson states at finite Reynolds numbers,'' Phys. Fluids A **5**, 2207 (1993).
[21] Y. Kondoh, M. Yoshizawa, A. Nakano, and T. Yabe, ''Self-organization of two-dimensional incompressible viscous flow in a friction-free box,'' Phys. Rev. E **54**, 3017 (1996).
[22] B. Jüttner, D. Marteau, P. Tabeling, and A. Thess, ''Numerical simulations of experiments on quasi-two-dimensional turbulence,'' Phys. Rev. E **55**, 5479 (1997).
[23] S. Li and D. Montgomery, ''Decaying two-dimensional turbulence with rigid walls,'' Phys. Lett. A **218**, 281 (1996).
[24] S. Li, D. Montgomery, and W. B. Jones, ''Inverse cascades of angular momentum,'' J. Plasma Phys. **56**, 615 (1996).
[25] S. Li, D. Montgomery, and W. B. Jones, ''Two-dimensional turbulence with rigid circular walls,'' Theor. Comput. Fluid Dyn. **9**, 167 (1997).
[26] H. J. H. Clercx, ''A spectral solver for the Navier-Stokes equations in the velocity-vorticity formulation for flows with two nonperiodic directions,'' J. Comput. Phys. **137**, 186 (1997).
[27] S. A. Orszag, ''Numerical methods for the simulation of turbulence,'' Phys. Fluids Suppl. II **12**, 250 (1969).
[28] P. M. Gresho, ''Incompressible fluid dynamics: some fundamental formulation issues,'' Annu. Rev. Fluid Mech. **23**, 413 (1991).
[29] H. J. H. Clercx, S. R. Maassen, and G. J. F. van Heijst, ''Spontaneous spin-up during the decay of 2D turbulence in a square container with rigid boundaries,'' Phys. Rev. Lett. **80**, 5129 (1998).
[30] G. F. Carnevale, J. C. McWilliams, Y. Pomeau, J. B. Weiss, and W. R. Young, ''Evolution of vortex statistics in two-dimensional turbulence,'' Phys. Rev. Lett. **66**, 2735 (1991).
[31] J. B. Weiss and J. C. McWilliams, ''Temporal scaling behavior of decaying two-dimensional turbulence,'' Phys. Fluids A **5**, 608 (1993).
[32] D. G. Dritschel, ''Vortex properties of two-dimensional turbulence,'' Phys. Fluids A **5**, 984 (1993).
[33] A. E. Hansen, D. Marteau, and P. Tabeling, ''Two-dimensional turbulence and dispersion in a freely decaying system,'' Phys. Rev. E. **58**, 7261 (1998).
[34] J. Weiss, ''The dynamics of enstrophy transfer in two-dimensional hydrodynamics,'' Physica D **48**, 273 (1991).